Boundary-Layer Meteorol (2009) 133:47–70
DOI 10.1007/s10546-009-9414-2

ARTICLE

The New Canadian Urban Modelling System: Evaluation for Two Cases from the Joint Urban 2003 Oklahoma City Experiment

Aude Lemonsu · Stephane Belair · Jocelyn Mailhot

Received: 20 August 2008 / Accepted: 3 August 2009 / Published online: 10 September 2009

Abstract A new Canadian numerical urban modelling system has been developed at the Meteorological Service of Canada to represent surface and boundary-layer processes in the urban environment. In this system, urban covers are taken into account by including the Town Energy Balance urban-canopy parameterization scheme in the Global Environmental Multiscale meteorological model. The new modelling system is run at 250-m grid size for two intensive observational periods of the Joint Urban 2003 experiment that was held in Oklahoma City, U.S.A. An extensive evaluation against near-surface and upper-air observations has been performed. The Town Energy Balance scheme correctly simulates the urban micro-climate, more particularly the positive nighttime urban heat island, and also reproduces the "cool" island during the morning but does not succeed in maintaining it during all of the daytime period. The vertical structure of the boundary layer above the city is reasonably well simulated, but the simulation of the nocturnal boundary layer is difficult, due to the complex interaction with the nighttime southerly low-level jet that crosses the domain. Sensitivity tests reveal that the daytime convective boundary layer is mainly driven by dry soil conditions in and around Oklahoma City and that the nighttime low-level jet reinforces the urban heat island in the first 300 m through large-scale advection, leading to the development of a less stable layer above the city.

Keywords Atmospheric boundary layer · Numerical simulation · Urban canopy model · Urban heat island

1 Introduction

The Meteorological Service of Canada has launched a program to improve the representation of cities in its mesoscale atmospheric numerical models with grid size from 20 km

A. Lemonsu (✉) · S. Belair · J. Mailhot
Meteorological Research Branch, Meteorological Service of Canada, Environment Canada, Dorval, QC, Canada
e-mail: aude.lemonsu@meteo.fr

down to about 200 m. An urbanized version of the Global Environmental Multiscale (GEM) meteorological model has thus been developed by including the Town Energy Balance (TEB) (Masson 2000) urban-canopy scheme in the surface module. The performance of the new urban modelling system is tested over Oklahoma City (referred to as OKC), Oklahoma, U.S.A. for two intensive observational periods of the Joint Urban 2003 field experiment (Allwine et al. 2004). The main goals of this evaluation are to examine: (1) the ability of the system to simulate the urban micro-climate (e.g., the air temperature at street level relevant to pedestrians), and (2) the impact of urban-scale surface fluxes (heat, humidity, momentum) on the dynamics of the daytime and nighttime atmospheric boundary layer.

The Joint Urban 2003 experiment is an interesting case to investigate because of the site's characteristics, as well as of the density and diversity of the observational networks. OKC is a medium size U.S. city with a typical downtown area composed of high-rise buildings and pre-dominant street orientations. The geographic situation of the city is rather simple (no maritime influence, homogeneous surroundings, and flat topography). However, a complication factor is that the Great Plains of the central U.S.A. are commonly crossed by a low-level jet (LLJ) that can be observed above OKC during summer. Thus, contrary to numerous studies that focus on calm situations, we propose to examine the OKC atmospheric boundary layer under consistent wind conditions, more especially at night. Because of the dense experimental system, including surface stations, radiosoundings, and wind profilers, the urban microclimate and local dynamics have been extensively documented during both nighttime and daytime.

Temperature measurements collected during the experiment display a positive urban heat island (UHI) (i.e., the low-level air temperature is greater above the city than above the countryside) during nighttime, varying between 2 and 4°C in accordance with that usually observed for U.S. cities (Bornstein and Lin 2000; Gedzelman et al. 2003; Fan and Sailor 2005; Fast et al. 2005; Rosenzweig et al. 2005). On the other hand, a negative UHI occurs during daytime, this trend being confirmed for the two periods studied herein. Other studies also show the occurrence of "cool" islands during the day (Pearlmutter et al. 1999; Bejarán and Camilloni 2003; Kim and Baik 2005; Chow and Roth 2006) that are usually more intense during summertime (Figuerola and Mazzeo 1998; Steinecke 1999). This effect is mainly due to the overshadowing of the urban canyons (Pearlmutter et al. 1999; Steinecke 1999), which is particularly the case for North American central business districts where buildings are very tall.

The Great Plains LLJ plays a key role in the regional dynamics, notably above the OKC area. Climatological studies indicate that it is mostly associated with strong horizontal pressure gradients (Bonner 1968), and frequently occurs at night, depicted predominantly from south to south-west (Bonner 1968; Helfand and Schubert 1995; Mitchell et al. 1995; Song et al. 2005). Its nose, i.e. its maximum wind speed, is observed to occur between 0600 and 1200 UTC and is located in the first 1,500 m, and can reach 10–25 $m\,s^{-1}$. According to Blackadar (1957), it is generated by an inertial oscillation that occurs after the nocturnal inversion develops, inducing a decoupling between the surface and the atmosphere. Previous work suggests the possible role of circulations caused by nighttime radiation cooling over sloping terrain (Bleeker and André 1951), and of topographic flow-blocking effects due to the Rocky Mountains (Peagle et al. 1984).

De Wekker et al. (2004) and Lundquist and Mirocha (2006) show that the nocturnal LLJ appears during most of the intensive observational periods (IOPs) of the Joint Urban 2003 experiment over Oklahoma City. The low-level jet generates turbulence by shear and can have a great influence on boundary-layer flow (Berg et al. 2004; Wang et al. 2005; Lundquist and Mirocha 2006). On the other hand, regular variations in wind speed and wind direction

are observed upwind, downwind, and inside the downtown core, suggesting the flow is also affected by the roughness of the city (Heap et al. 2004; Wang et al. 2005; Calhoun et al. 2007).

The first objective of our study is to evaluate the new Canadian urban modelling system using two episodes from the Joint Urban 2003 field experiment. The second objective is to investigate, using numerical experimentation, the possible impact that the urban environment has on the low-level jet often observed in this region. The experimental framework is first presented in Sect. 2 and is followed by a description of the modelling system and numerical set-up (Sect. 3). The overall model performance is investigated in the following two sections. More particularly, Sect. 5 focuses on the ability of the new system to simulate the urban micro-climate at street level and its variability according to different urban environments. Finally, Sects. 6 and 7 rely on numerical sensitivity experiments to provide understanding of the impact of the city on boundary-layer dynamics during both daytime and nighttime.

2 Experimental Framework

The Joint Urban 2003 field campaign (Allwine et al. 2004) is a large atmospheric dispersion study, and held in Oklahoma City (OKC), U.S.A., from June 28 to July 31, 2003. Located in the Great Plains region, at coordinates 35°23′ N, 97°36′ W, and 397 m above sea level, OKC is the most populous city of the state of Oklahoma with about 530,000 inhabitants, and is mainly composed of wide irrigated residential areas that extend around a relatively small central business district (CBD). The geographical surroundings of the city are homogeneous, with flat topography marked by a west-east gradient since the Rocky Mountains are located about 700 km to the west. The regional landscape is characterized by widespread grasslands, with mixed shrub and forest cover east of OKC. According to the climatological data provided by the World Weather Information service (http://worldweather.wmo.int/), the daily maximum and minimum temperatures during July are 34.1 and 21.4°C, respectively, and the mean monthly precipitation is 66 mm.

During the experiment, a dense network was deployed in and around the city to conduct tracer experiments and to document the atmospheric transport of contaminants. Numerous observational systems were used to document the meteorology in OKC during the experiment, and to provide insight into radiative, physical, and dynamical processes at regional and local scales. In addition to the observations that were continuously collected during the campaign, specific observations were performed during 10 IOPs, i.e., six during daytime and four during nighttime.

Three networks of sensors were installed around the city in order to document the urban micro-climate at street level. The Portable Weather Information Display Systems (PWIDS) network was composed of 15 stations located inside the CBD and provided measurements of air temperature, relative humidity, wind speed and wind direction. Thirteen of these sensors were mounted within streets at 8 m above ground level (a.g.l.), while two others were mounted on roofs. The so-called super PWIDS network comprised 20 stations also located inside the CBD, providing air temperature and wind components at 8-m height (some collocated with the PWIDS stations). Another network from the Pacific Northwest National Laboratory (PNNL) recorded temperature at 33 stations located at 3-m height along two 3-km long transects crossing the CBD and the surrounding suburbs from north to south and from east to west. The PWIDS and PNNL stations located in the CBD are presented in Fig. 1a. For the present study, only street-level measurements are analyzed, since those obtained at the roof tops can be considerably influenced by the roof itself.

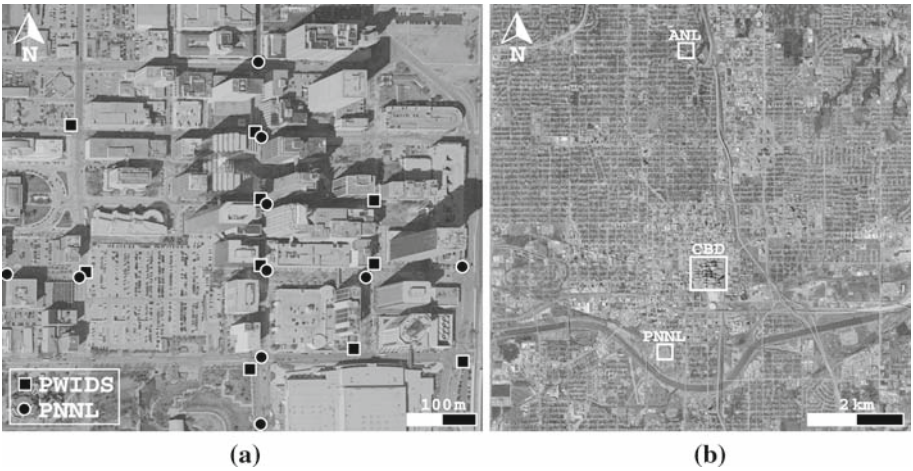

Fig. 1 **a** Urban networks of PWIDS and PNNL air temperature sensors located in the CBD at street level. **b** PNNL and ANL sites, including sodars, radars and radiosoundings, located upwind and downwind of the CBD, respectively

Two sites located south and north of the CBD were instrumented with sodars, radars and vertical soundings to characterize and compare the flow and thermodynamic structure of the boundary layer upwind and downwind of the CBD: the PNNL site, about 2 km south of the CBD, and the Argonne National Laboratory (ANL) site, almost 5 km north of the CBD (Fig. 1b). The sodars and radars worked continuously during the experiment, whereas the soundings were launched only during IOPs, i.e., between 0700 and 1600 local standard time (LST = UTC − 6) for the daytime IOPs, and between 2100 and 0600 LST during the nighttime IOPs.

3 Urban Modelling System Description

At the Meteorological Service of Canada, an urbanized version of the GEM mesoscale atmospheric model has been developed in order to improve the representation of surface and boundary-layer processes in the urban environment. This new system is used at grid scales between 200 m and 20 km. At such scales, the model does not explicitly resolve individual buildings but rather uses an urban parameterization, the TEB (Masson 2000) urban canopy model, which represents the physical mechanisms inside the urban canopy and the exchanges between the built-up covers and the atmosphere.

3.1 Urban Canopy Model

The TEB scheme is a single-layer urban canopy model based on a simplified three-dimensional geometry of the urban covers. The built-up areas are represented as an ensemble of urban canyons (Oke 1987) composed of roofs, roads, and walls with isotropic orientations. A set of mean geometric parameters, defined at each grid point, describes the urban canopy arrangement: building fraction, building height, canyon aspect ratio (i.e., ratio between building height and width of the street), and the ratio between walls and horizontal built-up areas. Radiative and thermal properties are associated with each urban facet. The energy balance is resolved independently for roads, roofs and walls by taking into account shadow effects

and radiation trapping inside the canyon. The turbulent exchanges inside the canyon, and between the canyon and the upper atmosphere, are determined using an aerodynamic resistance network with exchange coefficients that depend on wind speed and stability conditions. A mean urban micro-climate is resolved inside the canyon, and mean air temperature, mean specific humidity and mean wind speed obtained in the middle of the street at the mid-height of the buildings.

The TEB scheme has been extensively studied and evaluated both in offline and coupled modes for various urban areas such as the Mexico City core (Mexico) and the Vancouver light industrial area (BC, Canada) (Masson et al. 2002), Marseille (France) (Lemonsu et al. 2004, 2006a,b), Paris (France) (Lemonsu and Masson 2002; Sarrat et al. 2006), Toulouse (France) (Pigeon et al. 2007; Hidalgo et al. 2008). The scheme has not, however, been tested for a typical North American downtown area, such as OKC's central business district.

It should be noted that the TEB scheme is exclusively applied to the built-up covers. In mixed environments including a vegetation fraction, the scheme is coupled with a soil-vegetation-atmosphere transfer (SVAT) model that independently calculates the exchanges between the natural covers and the atmosphere. Contrary to more complex approaches, such as the urban model of Martilli et al. (2002), the atmospheric model does not directly interact with the urban canopy. In an approach similar to that in SVAT models, the first atmospheric level is located above the top of the buildings. Urban surface processes influence the atmospheric model through the surface fluxes of heat, humidity, and momentum.

3.2 Coupling with the Atmospheric Model

In the GEM model physics, the surface is described as a mosaic composed of four types of covers (or tiles): natural soils and vegetation, water, continental ice, and sea ice. For each tile, a specific surface parameterization is applied. The surface fluxes and boundary conditions required by the atmospheric model are then calculated at each grid point independently for the four tiles and averaged according to their respective cover fractions. Without urban parameterization, the effect of cities is represented in a crude manner using sandy soils with large roughness in the land-surface scheme. By including the TEB scheme in the GEM model, a new "urban" tile is added in the surface mosaic to take into account the built-up covers as an independent type of cover.

For the land-use land-cover description, the GEM model currently uses the 1-km global land-cover characteristics database (Loveland et al. 2000), regrouped into 26 land-use land-cover classes but with only one urban class, derived from the digital chart of the world (Danko 1992). To initialize and run the TEB scheme with spatial resolutions of a few hundreds of metres requires a finer description of urban areas. For this purpose, a new classification was developed by Lemonsu et al. (2006c), whose general methodology is based on the joint analysis of satellite imagery and digital elevation models. It provides a 60-m resolution of land-use land-cover classifications composed of 12 urban classes that characterize the variability of the urban landscapes. The TEB input parameters (geometric, radiative and thermal parameters) associated with each class were defined from aerial photograph analysis and the literature (Masson et al. 2002).

3.3 Numerical Set-up

In this study, the GEM model's numerical set-up is based on a one-way grid-nesting system of the limited-area version of the GEM model (i.e., GEM-LAM) cascading from 2.5- to 1-km

grid sizes, and from 1-km to 250-m grid sizes. Initial and boundary conditions for the 2.5-km GEM-LAM are provided by the 15-km operational GEM regional model (Mailhot et al. 2006).

The 2.5-km GEM-LAM configuration is very similar to an experimental version currently being tested at the Meteorological Service of Canada (Erfani et al. 2005), and includes 58 vertical levels based on a hybrid pressure coordinate up to 10 hPa, with 16 of these levels below 3,000 m. The lowest vertical level is located 50 m above canopy level. In the 1-km and 250-m GEM-LAM configurations, the vertical grid is composed of 53 levels. The vertical resolution has been increased near the surface (with more than twice the number of levels used in the 2.5-km model for the lowest 3,000 m), but stretched in the highest levels. In our version of the 2.5-km GEM-LAM, the condensation schemes are not activated and the turbulent mixing length is based on Lenderink and Holtslag (2004). Furthermore, the mixing length in the 250-m model is calculated using Blackadar (1962), for which the asymptotic mixing length depends on the cell size, i.e., $\lambda_0 = 0.23\sqrt{\Delta x \Delta y}$.

In addition to the TEB urban scheme, the surface module includes the Interaction Soil-Biosphere-Atmosphere (ISBA) SVAT model (Noilhan and Planton 1989) to represent surface exchanges between vegetation and atmosphere, which is already run operationally with the GEM regional and global models (Bélair et al. 2003). An early version of the Canadian Land Data Assimilation System (CaLDAS) (Balsamo et al. 2007) has been used to provide initial fields of soil water content and surface temperature to the 2.5-km GEM-LAM.

Two periods of the Joint Urban 2003 experiment were selected for this study: (1) IOP6, which took place during daytime on July 16 2003, and (2) IOP9, which took place during the night between July 26 and 27 2003. Both IOPs correspond to clear sky episodes during which the near-surface air temperature peaked at about 35°C during the day and decreased to about 24°C at night. A south-westerly to southerly flow was observed during daytime, with a strong nocturnal south-westerly LLJ at night.

The integration domains are presented in Fig. 2. The 2.5- and 1-km GEM-LAM versions are integrated over 200 × 200 grid point domains centered on OKC. For the 250-m GEM-LAM, an integration domain that is too small does not allow for the realistic development of the turbulence around and over the city because of the influence of the lateral boundaries. To avoid this problem, the 250-m GEM-LAM was operated using a 200 × 400 grid that is oriented according to the mean flow direction, with the extension upwind of the city.

The characteristics of the numerical integrations are summarized in Table 1. For IOP6, the 2.5-km, 1-km, and 250-m GEM-LAM models are integrated for 33, 24, and 21 h, respectively, by applying a systematic time lag between consecutive simulations. For IOP9, the integrations are 30, 24, and 21 h long. Two types of simulations are performed in order to quantify the impact of the new urban parameterization: (1) *No Urban* is a simulation without specific representation of urban covers, i.e., without the TEB scheme and for which the urban class is replaced by vegetation. For OKC, the city is converted into grassland corresponding to one of the main types of covers that are found in the region; (2) *Urban* is a simulation that includes the TEB scheme and uses the new urban land-use land-cover classification.

4 Regional-Scale Evaluation

A regional-scale evaluation is first done in order to estimate the model's ability to simulate the synoptic situation and to verify its ability to reproduce the nocturnal LLJ observed across the Great Plain regions. For this purpose, the 2.5-km GEM-LAM fields are compared with observations from the Oklahoma MESONET surface operational network

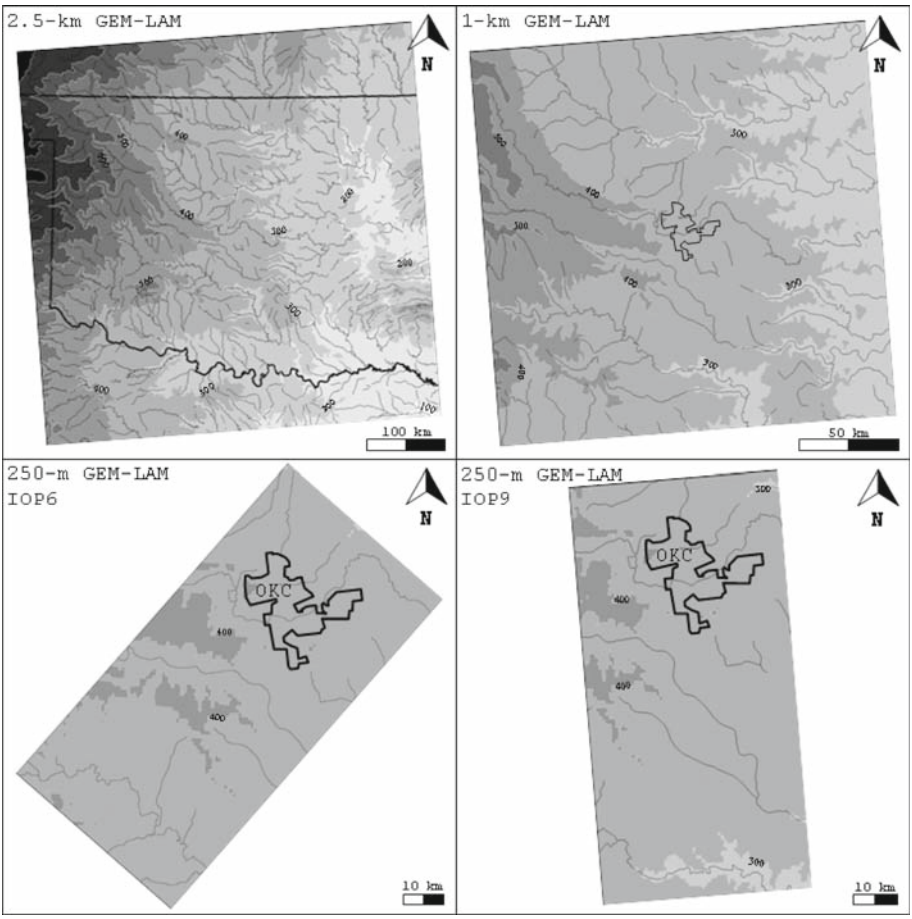

Fig. 2 Numerical set-up for the IOP6 and IOP9 integrations. The 250-m GEM-LAM domains are differently oriented for IOP6 (*bottom left*) and IOP9 (*bottom right*) according to the mean flow. The *black line* indicates the limits of OKC

Table 1 Description of the numerical set-up

Model	Res. (km)	Grid	Initial time	Duration (h)
IOP6				
GEM regional	15	Global	16 July, 0000 UTC	42
GEM-LAM	2.5	201 × 201	16 July, 0600 UTC	33
GEM-LAM	1	201 × 201	16 July, 0900 UTC	24
GEM-LAM	0.25	401 × 201	16 July, 1200 UTC	21
IOP9				
GEM regional	15	Global	26 July, 0000 UTC	36
GEM-LAM	2.5	201 × 201	26 July, 0600 UTC	30
GEM-LAM	1	201 × 201	26 July, 1200 UTC	24
GEM-LAM	0.25	201 × 401	26 July, 1500 UTC	21

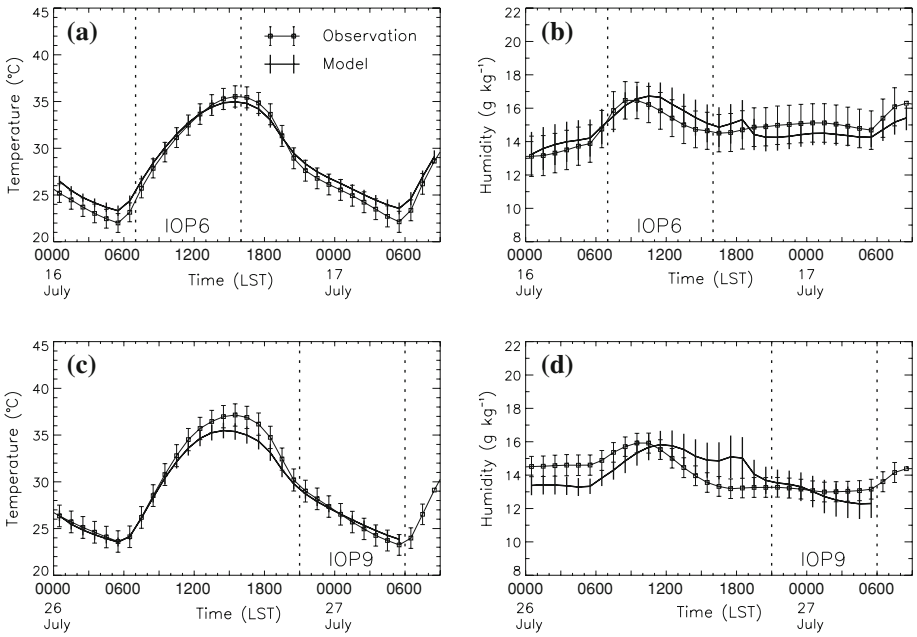

Fig. 3 Evaluation of 2.5-km GEM-LAM against operational MESONET stations: comparison of simulated and observed air temperature (*left*) and specific humidity (*right*) near the surface for IOP6 (*top*) and for IOP9 (*bottom*). The *black* and *grey vertical bars* represent the standard deviation associated with simulated and observed averaged data, respectively

(http://www.mesonet.ou.edu/) and with the Norman (NRM) radiosounding, located almost 30 km to the south of the OKC CBD. Since the MESONET stations and the Norman sounding are all in rural locations, *Urban* and *No Urban* provide very similar results for these areas. In this section, only results from the *Urban* 2.5-km integration are presented and compared to observations.

4.1 Near-Surface Parameters

The 86 stations of the Oklahoma MESONET, located inside the 2.5-km GEM-LAM integration domain (500×500 km^2), are used for the comparison. Simulated near-surface air temperature and specific humidity are valid at 1.5 m above the top of the canopy and are obtained using stability functions based on Delage and Girard (1992) and Delage (1997). They are interpolated from the model grid to the locations of the stations. The results are averaged for the 86 stations and averaged in time using a 1-h timestep. The comparisons performed for IOP6 and IOP9 show good performance of the model, and for IOP6 (Fig. 3a, b), air temperature and specific humidity are very well simulated during daytime. During nighttime, however, air temperature is systematically overestimated by 1.0–1.5°C. Figure 3a, b indicate that this bias is correlated with a slight underprediction of specific humidity. For IOP9 (Fig. 3c, d), the simulated nighttime air temperature is in very good agreement with observations. The daytime air temperature is underpredicted and associated with an overestimation of specific humidity.

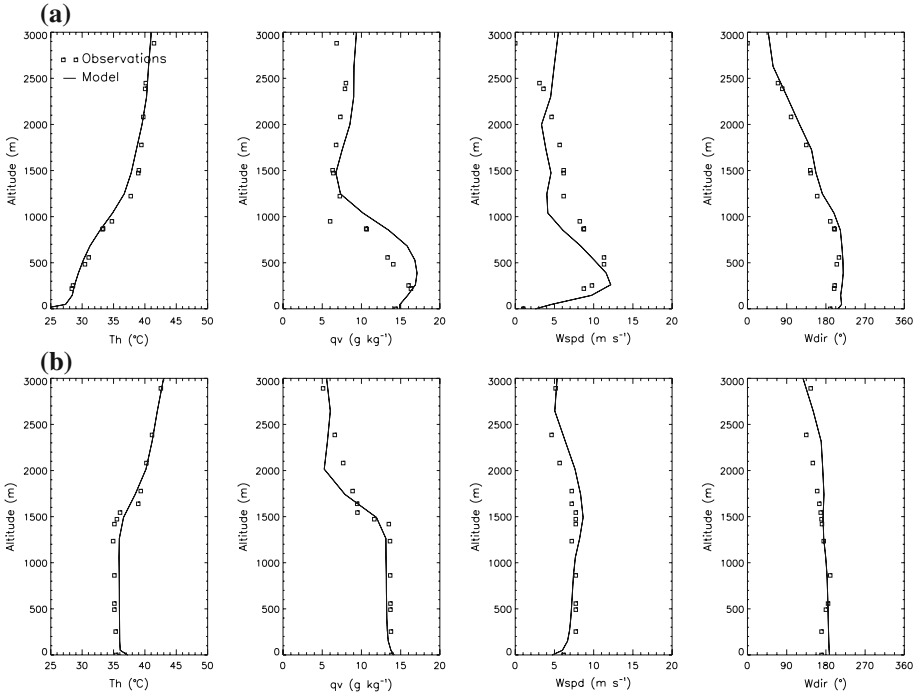

Fig. 4 Evaluation of the 2.5- km GEM-LAM against Norman's sounding for IOP6: comparison of simulated (*solid line*) and observed (*squares*) vertical profiles of potential temperature, specific humidity, wind speed, and wind direction on July 16 at 0600 LST (*top*) and 1800 LST (*bottom*)

4.2 Upper-Air Profiles

Figures 4 and 5 display vertical profiles of potential temperature, specific humidity, wind speed, and wind direction observed at NRM located 30 km south of OKC. As can be seen, model results compare relatively well against observations for the two IOPs.

The 0600 LST NRM soundings (Figs. 4a, 5b) confirm the occurrence of a nocturnal LLJ for the two episodes, in accordance with De Wekker et al. (2004) and Lundquist and Mirocha (2006). Its characteristics are, however, different for the two IOPs. During IOP6, the LLJ orientation is from the south-south-west, but is from the south-west during IOP9. The wind speed profiles indicate that the LLJ is stronger and deeper during IOP9; it does not extend above 1,100 m in IOP6 with a wind-speed maximum reaching about 12 m s^{-1}, whereas the maximum exceeds 16 m s^{-1} in IOP9 with a vertical extent of 2,000 m. These two situations are well depicted by the model. During both IOPs, the observed 0600 LST profiles underscore a strong cooling at the surface with a mixed layer above. This mixed layer is about 1,000 m deep for IOP6 (Fig. 4a), which is slightly overpredicted by the model, but is more extended for IOP9 both in observations and model results (Fig. 5b). During daytime (1800 LST sounding), a well-mixed layer of 1,600-m depth is observed and simulated during IOP6 (Fig. 4b), associated with a southerly flow of 6–8 m s^{-1}. The wind conditions are similar during IOP9 but the boundary layer reaches at least to 2,500 m in this case (Fig. 5a). Again, the model performs well, although the specific humidity is overestimated by approximatively

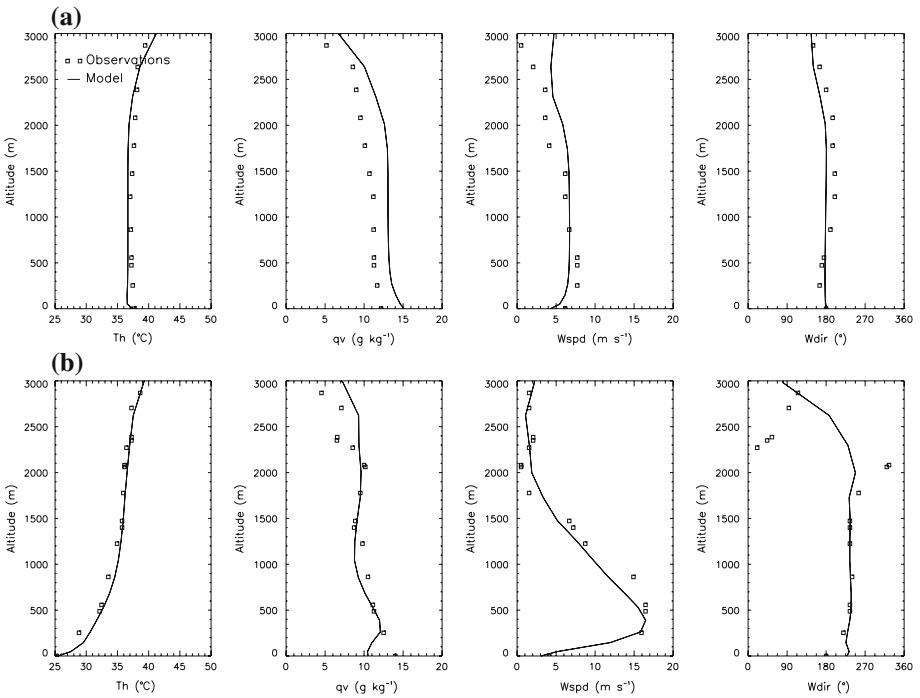

Fig. 5 Evaluation of 2.5-km GEM-LAM against Norman's sounding for IOP9: comparison of simulated (*solid line*) and observed (*squares*) vertical profiles of potential temperature, specific humidity, wind speed, and wind direction on July 26 at 1800 LST (*top*) and on July 27 at 0600 LST (*bottom*)

$2\,\mathrm{g\,kg^{-1}}$. This error, however, is considerably reduced in the higher resolution simulations (not shown here).

5 Urban Microclimate

This section first presents an analysis of the city core microclimate using stations exclusively installed in the CBD. The variability of the urban microclimate is then investigated by comparing observed and simulated air temperatures at various locations in the city.

5.1 Central Business District Microclimate

An observed mean air temperature T_{URB_o} was derived from the 13 PWIDS stations installed in street canyons inside the CBD (see Fig. 1a), and compared to T_{URB_m} which was calculated from the 250-m GEM-LAM results. In order to evaluate the urban heat island (UHI) at street level, a subset of 11 MESONET stations located in the rural areas immediately surrounding OKC (from 30 to 80 km away from the CBD) was selected for the computation of the mean rural air temperature T_{RUR_o} (in contrast to the set of 86 MESONET stations used for regional-scale evaluation in Fig. 3a, c). The averaged simulated temperature T_{RUR_m} was diagnosed using the 2.5-km GEM-LAM results because the 250-m integration domain is too small to contain a sufficient number of MESONET stations in the rural environment around OKC.

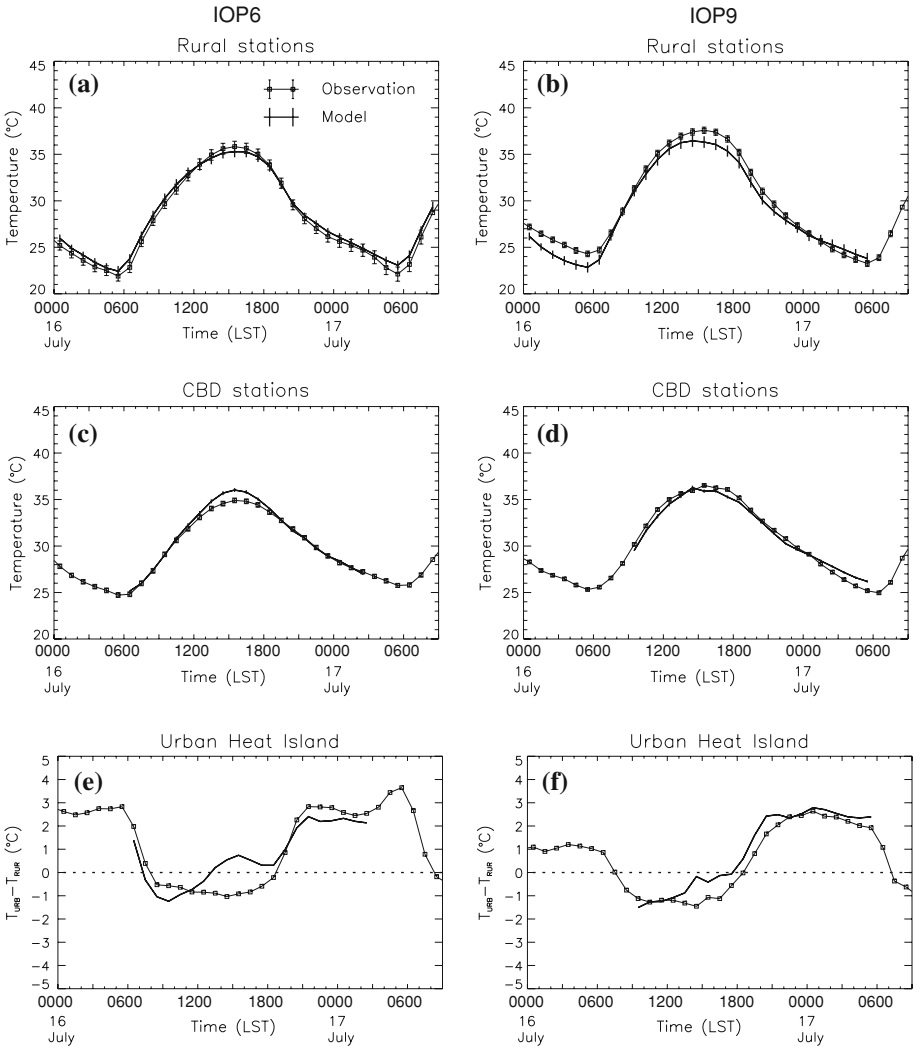

Fig. 6 Evaluation of the urban microclimate simulated by 250-m GEM-LAM for IOP6 (*left*) and IOP9 (*right*): comparison of simulated and observed air temperature in rural environment (*top*) using 11 MESONET stations located around OKC, in the CBD (*middle*) using PWIDS stations, and comparison of simulated and observed UHI (*bottom*)

Figure 6 presents the observed and simulated air temperatures for the two IOPs, as well as the UHI computed as $T_{RUR} - T_{URB}$. For IOP6, T_{RUR_m} is in very good agreement with observatios. For IOP9, the air temperature is underestimated by about 1.5°C during the first night and during daytime, but is very well predicted for the second night. The street-level air temperature inside the CBD is well predicted by the model for the two cases, except for a 1°C overestimation for the daytime temperature maximum during IOP6. The small positive bias observed during the IOP9 nighttime period seems to be associated with the slight overestimation already observed at the regional scale.

As expected, the amplitude of the air temperature diurnal cycle is smaller in the city than in the surrounding rural environment. This effect is well reproduced by the model, and in particular, there is a rapid nocturnal cooling observed outside the city after 1800 LST, with the cooling much less in the CBD. The *Urban* simulation depicts well this effect, as well as the development of the nocturnal UHI that reaches about 2.5°C between 2100 and 0600 LST. During daytime, air temperature is lower in the CBD than in the surrounding countryside, inducing a negative UHI between 0800 and 1800 LST of almost −1°C in IOP6 and of just over −1°C in IOP9. For the two IOPs, the model succeeds in predicting this negative UHI in the morning, but the temperature difference between rural and urban environments rapidly decreases during the day. The IOP6 results (Fig. 6, left panel) indicate that the simulated UHI even becomes positive at 1500 LST, i.e., at the daytime temperature maximum.

Some hypotheses can be proposed in order to explain the difficulty of the model in predicting a systematically negative UHI through the daytime, given that this disagreement appears to be linked to an overestimation of the street-level air temperature increase. First, temperatures from the model simulations and the observations are not exactly comparable. Based on several simplifying numerical assumptions, the TEB scheme predicts a mean air temperature inside the streets at the mid-height of buildings (thus varying according to building height) and at the mid-distance of the walls without considering street intersections. In contrast, the temperature sensors are all located 8 m a.g.l. at street intersections. Moreover, the TEB scheme uses for radiative and turbulent calculations the mean building heights (at 250-m spatial resolution) that may be underestimated in comparison with the real height of the buildings that locally surround the PWIDS stations. These two particularities of the urban canopy model probably tend to predict a greater incident radiation received by the system than that actually received by the sensors, which consequently leads to greater warming inside the streets.

5.2 Urban Microclimate Variability

The PNNL surface stations were installed along two perpendicular north-south and east-west streets (presented in Sect. 2) that were representative of several types of urban environments: (1) the CBD, which is located at the intersection of the two streets, is a very densely built-up area composed of tall skyscrapers (see aerial picture in Fig. 1a); (2) the areas that surround the CBD mostly correspond to commercial and business areas with almost no vegetation (the buildings are, however, lower than in the CBD); and (3) the most distant districts are mostly industrial sectors composed of natural soils, parking lots and large, but low, buildings. The 33 PNNL stations are regrouped according to these three different urban classes, referred to as *CBD* (6 stations), *Commercial* (13 stations), and *Industrial* (14 stations), respectively. These urban landscapes can be differentiated in the model using the new urban land-use land-cover classification presented in Sect. 3.2. Different TEB input parameters are associated with the different urban classes. More specifically, the mean building height is 40, 25, and 8 m for the *CBD*, *Commercial*, and *Industrial* classes respectively, with aspect ratios of 2.0, 1.1, and 0.3. Thermal and radiative properties are also different for *Industrial*, which is mainly composed of warehouses (based on Masson et al. 2002).

Observed and simulated air temperatures from IOP6 for the three urban classes are presented in Fig. 7 (those from IOP9 are similar), which also shows the UHI recomputed for the three urban classes using the same rural stations as in Sect. 5.1. The diurnal cycles of temperature and UHI are quite similar for the *CBD*, *Commercial*, and *Industrial* areas. That for the *CBD* stations, however, indicates a daytime maximum always lower than those observed in the two other urban environments, a feature that is also well captured by the model.

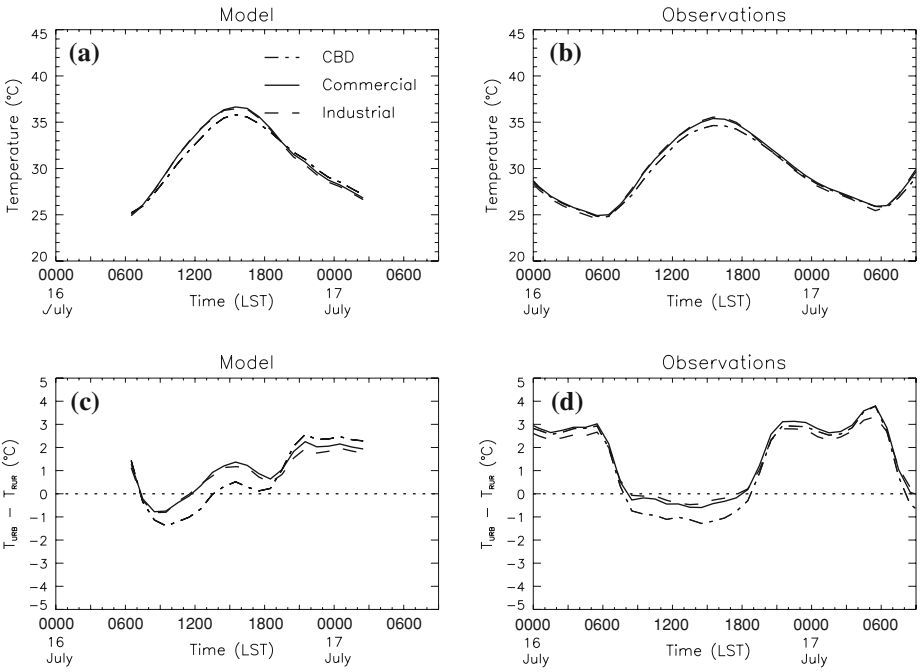

Fig. 7 Evaluation of the urban microclimate variability simulated by 250-m GEM-LAM for IOP6: comparison of simulated (*left*) and observed (*right*) air temperature (*top*) and UHI (*bottom*) for three different urban environments using PNNL stations

The daytime warming is limited, probably due to the geometric characteristics of the CBD: the buildings are very tall, which reduces the penetration of the incident radiation inside the streets. A negative UHI consequently develops at daytime, as already underlined by the PWIDS stations that are located in the same area (Fig. 6). For the *Commercial* and *Industrial* stations, a negative UHI is also observed (and simulated in the first daytime hours) but remains weaker, i.e., less than 0.5°C. At night, the *Commercial* stations record the highest air temperatures, with the lowest ones observed at the *Industrial* stations.

It is interesting to note that the simulations provide distinct urban microclimates for the *CBD*, *Commercial*, and *Industrial* classes. During daytime, the simulated air temperature is lower at the *CBD* stations than at the *Commercial* and *Industrial* stations by almost 1°C, which is similar to that observed (Fig. 7). This specific behaviour is strongly driven by the geometric parameters that are defined in the CBD. In the simulation, the very high density of built-up surfaces in this region leads to less nocturnal cooling although the observations indicate that the *Commercial* region remains slightly warmer at night. This difference can be related to other effects or parameters, such as the material properties, but, even so, the model indicates, in agreement with observations, that the *Industrial* areas are systematically cooler at night, probably due to the presence of vegetation.

6 Daytime Urban Effects

We now discuss the impact of the city on the vertical structure of the boundary layer during both daytime (IOP6) and nighttime (IOP9). For this purpose, observed and simulated

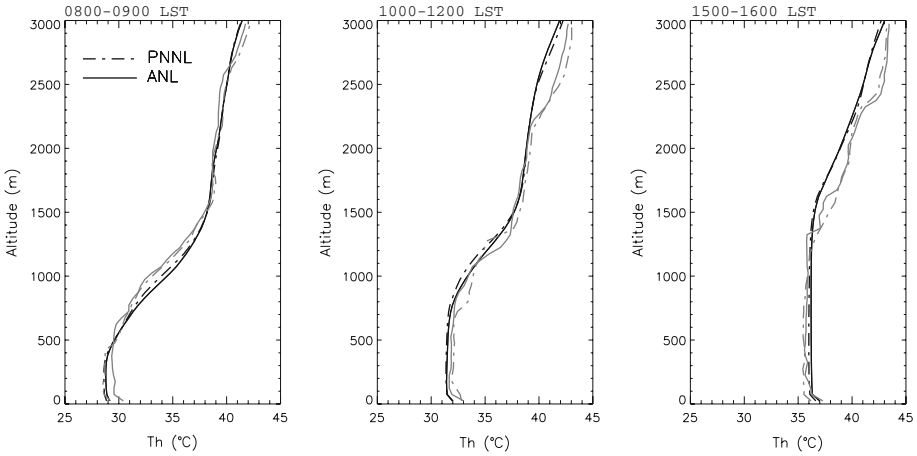

Fig. 8 Comparison of simulated and observed potential temperature vertical profiles at ANL and PNNL using radiosounding data for IOP6. The vertical profiles are temporally averaged on the periods 0800–0900 LST (*left*), 1000–1200 LST (*middle*), and 1500–1600 LST (*right*) on July 16. *Black* and *grey lines* refer to model and observations, respectively

upper-air profiles, upwind and downwind of the CBD, are examined. An analysis of numerical sensitivity experiments (*Urban* and *No Urban* simulations mentioned in Sect. 3.3) is presented to evaluate not only the urban effects but also to investigate the city's interactions with the LLJ larger-scale circulation during IOP9 (discussed further in Sect. 7).

6.1 Urban Upper-Air Profiles

Vertical profiles of potential temperature from the 250-m GEM-LAM are compared with soundings at PNNL and ANL. Both stations are located in residential districts inside OKC's urban area, south and north of CBD, respectively (Fig. 1b). Figure 8 shows the observed and simulated profiles averaged for the periods 0800–0900, 1000–1200, and 1500–1600 LST on July 16. The soundings show the progressive warming of the convective boundary layer from 0800 to 1600 LST, as well as its vertical extension. The boundary layer is well mixed in the lowest 400 m at 0800–0900 LST, reaches 700–800 m at 1000–1200 LST and then approximately 1,300 m at 1500–1600 LST. From the potential temperature profiles, the model correctly simulates the diurnal development of the boundary layer at ANL and PNNL despite a slight overprediction of boundary-layer height at 1500–1600 LST.

The comparison between the two locations does not underline obvious and significant differences during daytime in both observations and simulations. This comparison is difficult because of the complex multi-layer vertical thermal structure, particularly at ANL. Besides, although the data have been averaged temporally, the measurements are made at fixed locations and no spatial averaging is done. Considering the dry soil conditions in the region and the high air temperatures, strong turbulent updrafts and downdrafts develop above and around the city during daytime and randomly affect the sounding measurements.

6.2 Impact of the City on Boundary-Layer Structure

Figure 9 presents the temporal evolution, from 0900 to 1900 LST, of the difference between the potential temperature profiles simulated by *Urban* and *No Urban* ($\Delta\theta = \theta_{Urban} - \theta_{No\ Urban}$) above the CBD (computed for a 500 m × 500 m grid). Before 1400 LST,

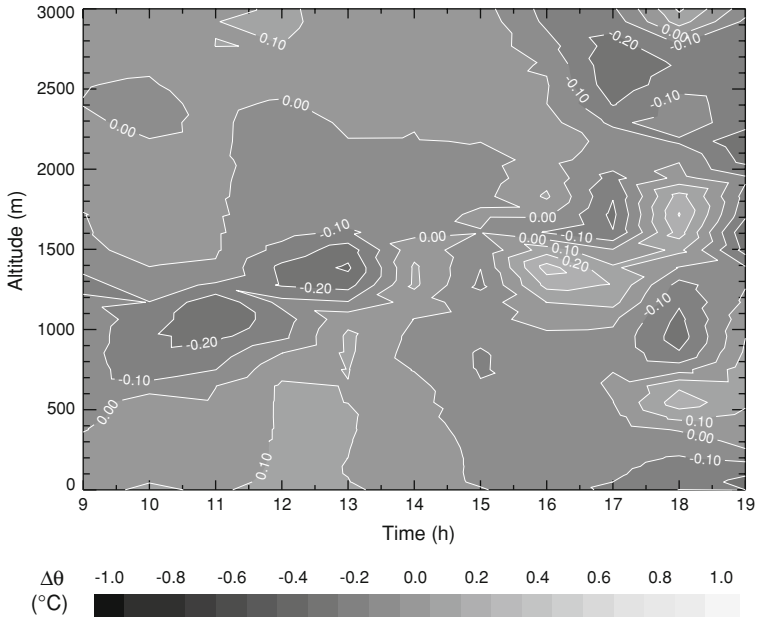

Fig. 9 Temporal evolution (from 0900 to 1900 LST on July 16) of the difference between potential temperature vertical profiles simulated by *Urban* and *No Urban* above the CBD ($\Delta\theta = \theta_{Urban} - \theta_{No\ Urban}$)

negative anomalies are noted at the top of the growing boundary layer, resulting from the fact that the boundary layer is slightly higher in *Urban* than in *No Urban*. The convective boundary layer develops and warms more rapidly above the urban cover in the morning. At 1500 LST (corresponding to the daytime temperature maximum), both simulations produce a similar boundary layer. In the afternoon, in contrast to the morning, it seems that the boundary-layer height decreases earlier in *Urban* and the boundary layer is slightly cooler. All these temperature differences are, however, quite small and do not exceed 0.2°C. The sensitivity tests conducted for IOP6 during daytime do not indicate a significant influence of the city on the vertical structure of the atmosphere and on the local circulations. This summertime period is characterized by large temperature maxima and low soil water content for the while region. These conditions favour the turbulence production over natural soils that surround OKC and consequently limit the impact and role of the city.

7 Nighttime Urban Effects

7.1 Urban Upper-Air Profiles

For IOP9, potential temperature, wind speed, and wind direction profiles at PNNL and ANL are compared with GEM-LAM 250-m fields, both averaged for the time periods 2100–2200, 0100–0400, and 0500–0600 LST (Fig. 10). At 0600 LST, the NRM operational sounding located 30 km south of the CBD in a purely rural environment is also available (presented in Fig. 5). From 2100 to 0600 LST, the soundings display, what we refer to as, a "less stable" layer (i.e., a shallow layer in the lowest 200 m of the atmosphere characterized by a lower static stability than the layer above) that is capped by a nocturnal inversion at both ANL and

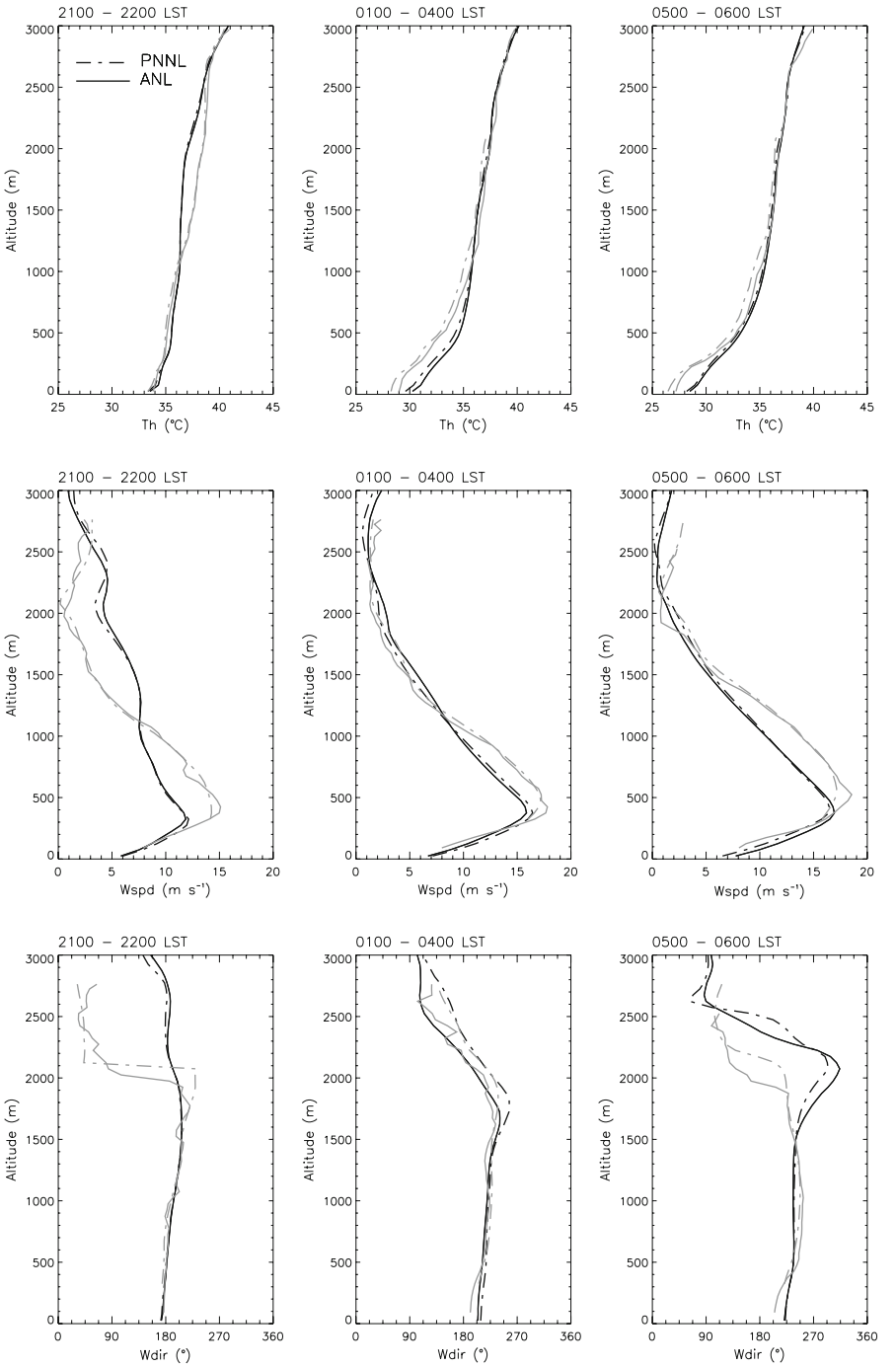

Fig. 10 Comparison of simulated and observed potential temperature (*top*), wind speed (*middle*), and wind direction (*bottom*) vertical profiles at ANL and PNNL using radiosounding and radar data for IOP9. The vertical profiles are temporally averaged on the periods 2100–2200 LST (*left*) on July 26, 0100–0400 LST (*middle*), and 0500–0600 LST (*right*) on July 27. *Black* and *grey lines* refer to model and observations, respectively

PNNL. As the night progresses, this "less stable" layer persists and even extends up to 300 m, while strongly cooling, thus reinforcing the inversion above. This process may contribute to the intensification of the nocturnal LLJ. Radar profiles clearly show that the wind speed maximum increased to about 17 m s^{-1}, and its location rose up to about 500 m at 0500–0600 LST. According to the wind direction profile, a progressive rotation of the LLJ from south to south-west occurred during the night. A strong shear (characterized by a sudden wind shift from south/south-west to east/north-east) appeared above the LLJ at about 2,000 m, and a decoupling also emerged between the LLJ and the near-surface layer where the flow still remained oriented from south or south-south-east. As with the daytime situation (Sect. 6.1), the atmosphere above OKC presents a multi-layer structure due to the complex flows in the area.

Comparison of ANL and PNNL soundings clearly indicates a positive temperature gradient from south to north of the CBD, corresponding to a warming of the flow across the city. These results are in agreement with De Wekker et al. (2004): by averaging all IOPs nighttime radiosoundings, they showed a tendency towards a higher temperature at ANL than at PNNL, especially in the first 150 m. The NRM sounding (Fig. 5b, left panel) confirms that the temperatures are even lower upwind of the city. In addition, the low-level jet is stronger at ANL and slightly shifted to the west, which is also consistent with De Wekker et al. (2004).

The simulated profiles display the development of a shallow layer in the first 300 m of the atmosphere both at PNNL and ANL. This layer is however less mixed and its cooling is less rapid than that indicated by the soundings between 0100 and 0600 LST, leading to an overprediction of 2°C of the surface-layer temperature. In addition, the development of the simulated nocturnal LLJ is late in comparison with the observations, and consequently its wind-speed maximum is underestimated at 2100–2200 LST, whereas the strong decrease of the wind speed above the LLJ's nose displayed by the radars is less marked in the simulated profiles. For the other two periods, when the flow is well developed, the LLJ remains slightly underestimated but the location of its maximum, as well as its direction and its vertical extent, are correctly simulated. The near-surface characteristics, however, indicate that the wind speed is slightly overestimated and that the wind rotation observed in the first 200 m is not well reproduced. Finally, it is interesting to note that the model is able to simulate the temperature gradient between PNNL and ANL.

7.2 Interaction Between the Urban Heat Island and Large-scale Circulations

A strong and well established UHI is observed and simulated at canopy level between 1900 and 0600 LST (Sect. 5.1). In this section, the vertical structure of the UHI and its impact on the boundary layer are discussed using numerical sensitivity experiments. Figure 11 shows the nighttime evolution of the vertical profile of $\Delta\theta = \theta_{Urban} - \theta_{No\ Urban}$ above the CBD, where positive values of $\Delta\theta$ indicate warming due to urban effects alone. The impact of the city is maximum in the evening and its maximum vertical extent reaches 200 m; during the night, the temperature difference decreases as does its vertical extent. By sunrise, the urban effect becomes quite small above 100 m, with $\Delta\theta$ less than 0.4°C.

Results from the GEM-regional model indicate that large-scale circulations also contribute to horizontal temperature gradients in the Great Plains region (Fig. 12). A southerly flow from the Gulf of Mexico meets with a northerly flow to produce a strong convergence zone at the northern border of Kansas in the afternoon until 2300 LST. A south-north temperature gradient results from this circulation. At night, the southerly flow progressively rotates to the west, reducing the convergence effect and the horizontal temperature gradient.

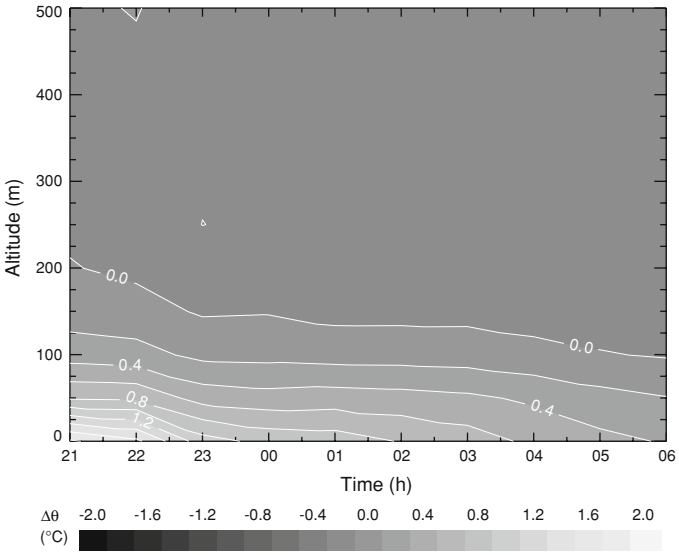

Fig. 11 Temporal evolution (from 2100 LST on July 26 to 0600 LST on July 27) of the difference between potential temperature vertical profiles simulated by *Urban* and *No Urban* above the CBD ($\Delta\theta = \theta_{Urban} - \theta_{No\ Urban}$)

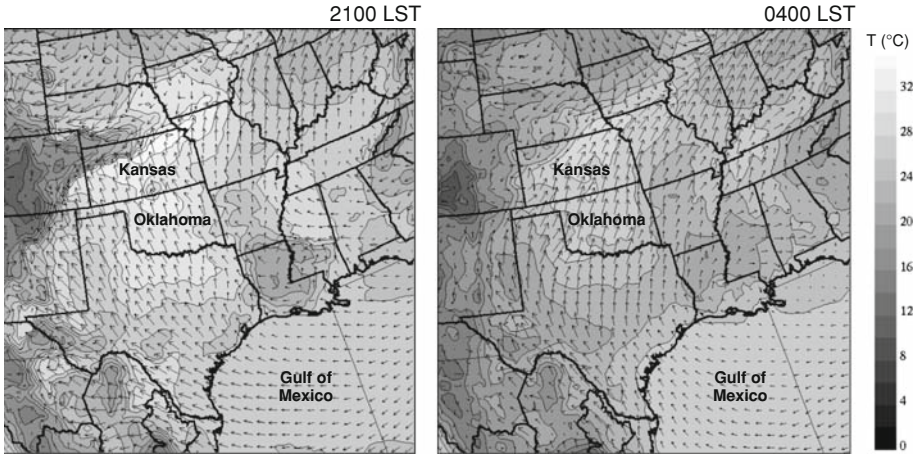

Fig. 12 Low-level large-scale circulations over the Great Plains region from the GEM-regional model: temperature and wind at 250 m a.g.l. on July 26 at 2100 LST and on July 27 at 0400 LST

Nevertheless, the development of the nocturnal LLJ and its intensification during the course of the night tend to reinforce the horizontal temperature gradient after 0200 LST.

At the scale of the greater OKC area, these circulations contribute to the horizontal temperature differences observed by the soundings located upwind and downwind of the CBD (Sect. 7.1, Fig. 10), i.e. higher air temperatures in the northern part of the domain. In order to separate the urban and large-scale effects, a potential temperature anomaly ($\Delta\theta_a$) is computed at each vertical level as the difference between the mean potential temperature above

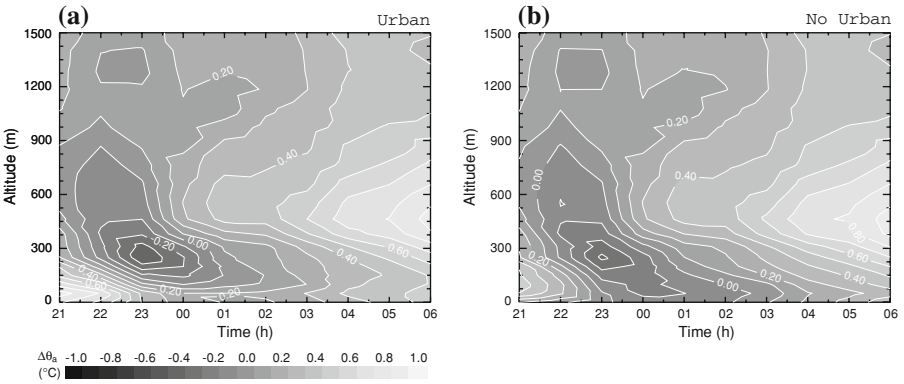

Fig. 13 Temporal evolution of vertical profile of potential temperature anomaly during the nighttime period of IOP9 for the two simulations *Urban* (*left*) and *No Urban* (*right*)

the OKC urban areas and the mean potential temperature above the southern part of the domain. The temporal evolution of the $\Delta\theta_a$ vertical profile between 2100 and 0600 LST is shown in Fig. 13 for the two simulations *Urban* and *No Urban*. Both *Urban* and *No Urban* produce positive values of $\Delta\theta_a$ associated with the southerly wind regime during the evening and with the nocturnal LLJ during the night. Between these two periods, there is a transition period with a negative anomaly at 300 m above canopy level reaching -0.3 K. Note that $\Delta\theta_a$ estimated from the simulation *No Urban* results from the large-scale circulations only. In this case, the nocturnal LLJ induces a warming effect that increases with altitude and with wind speed, up to about 450 m, which corresponds to the location of the LLJ wind-speed maximum (Figs. 10, 13). This positive anomaly also increases during the night as the LLJ intensifies. The simulation case *Urban* illustrates the coupling between urban effects and the nocturnal LLJ. In contrast to the *No Urban* case, a systematic positive anomaly occurs close to the surface even during the transition period between the two regimes because the urban effects are preponderant in this case. In addition, in the first 300 m above the canopy level, the UHI reinforces the warming effect associated with the horizontal temperature gradient that is generated by the nocturnal LLJ. This leads to a homogeneous $\Delta\theta_a$ throughout this layer.

7.3 Impact of the City on the Nocturnal Low-Level Jet

The nocturnal LLJ becomes evident between 2000 and 2100 LST and diminishes after 0600 LST. Figure 14 shows north-south vertical cross-sections of the difference between the simulated horizontal wind speed from the *Urban* and from the *No Urban* simulations at 2200 and 0400 LST. The wind-speed difference ($\Delta U = U_{Urban} - U_{No\ Urban}$) exhibits negative values near the surface, reflecting the fact that *Urban* systematically predicts weaker winds in the first 300 m due to the deceleration caused by the greater roughness of the city (Fig. 14a, b). This effect was also underlined by Liu et al. (2006) using numerical simulations with the fifth-generation Pennsylvania State University NCAR Mesoscale Model (MM5) including a simple parameterization of urban cover. Important wind-speed differences are also noted to the north of the CBD between 200 and 250 m above canopy level, which are linked to the flow pattern simulated by *Urban* at 2200 LST, and which extends to higher levels above and downstream of the city (with a slightly lower maximum wind speed than in *No Urban*). The impact of the city on the LLJ maximum wind speed is also underlined by Fig. 15, which

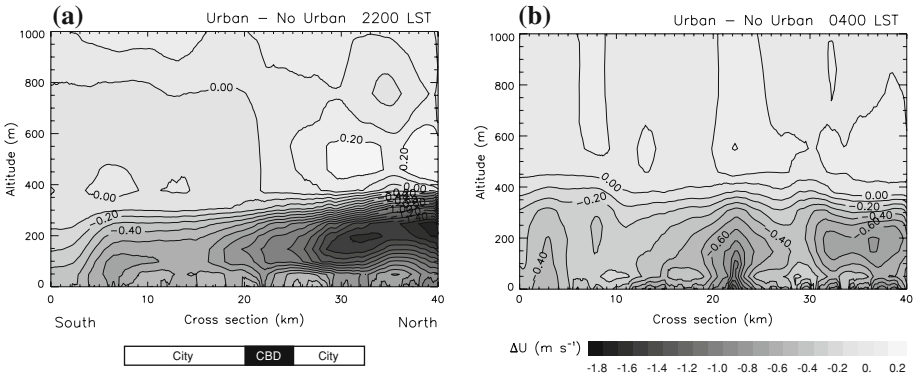

Fig. 14 North-south vertical cross section of the difference between horizontal wind speed simulated by *Urban* and *No Urban* ($\Delta U = U_{Urban} - U_{No\ Urban}$) on July 26 at 2200 LST (*left*) and on July 27 at 0400 LST (*right*). *Black* and *white rectangles* (bottom of left cross section) represent the site of the city and the CBD, respectively, along the transect

shows the difference between the maximum horizontal wind speeds simulated by *Urban* and *No Urban* at 2200 LST. The difference is about -0.2 or $-0.3\,\mathrm{m\,s^{-1}}$ above the most urbanized areas and reaches $-0.6\,\mathrm{m\,s^{-1}}$ downstream (i.e., north of OKC). The vertical resolution is insufficient to accurately simulate the effect of the city on the location of the LLJ maximum in altitude. The cross-section displays a rise of the flow from 50 to 100 m, the maximum effect being observed downwind of the city. At 0400 LST, the urban effects are much weaker even if a slight deceleration coupled to a small rise are still observed downstream (not shown).

8 Summary and Conclusions

A new urban modelling system including the TEB urban scheme has been developed at the Meteorological Service of Canada in order to improve the representation of cities in the Canadian mesoscale atmospheric models. This system is evaluated over Oklahoma City within the framework of the Joint Urban 2003 experiment. Numerical results from the 250-m GEM-LAM for two different intensive observation periods show that TEB's implementation leads to a more realistic prediction of temperature variations for various urban environments. The model is able to reproduce the systematic positive nocturnal UHI, as well as the negative UHI in the morning. However, it does not succeed in maintaining the negative UHI during the entire daytime period as observed, which could be explained by limitations in the radiative calculations associated with the simplified representation of the urban canopy in the TEB scheme. The complexity and heterogeneity of the urban landscape in OKC's city core, but also the particular locations of meteorological stations at street intersections, make it difficult to accurately simulate air temperature at street level. Nevertheless, considering our scientific objectives and the targeted spatial resolutions, the present performance of the new urban modelling system for the prediction of street-level microclimate is very encouraging. The main patterns are well simulated and the sensitivity results underline the considerable improvement brought by the inclusion of a specific urban-canopy parameterization.

Upper-air profiles and numerical sensitivity experiments indicate that the impact of urban covers on the vertical structure of the lower atmosphere does not remain significant for the entire day. The turbulence related to large surface heat fluxes, themselves due to the dry soil

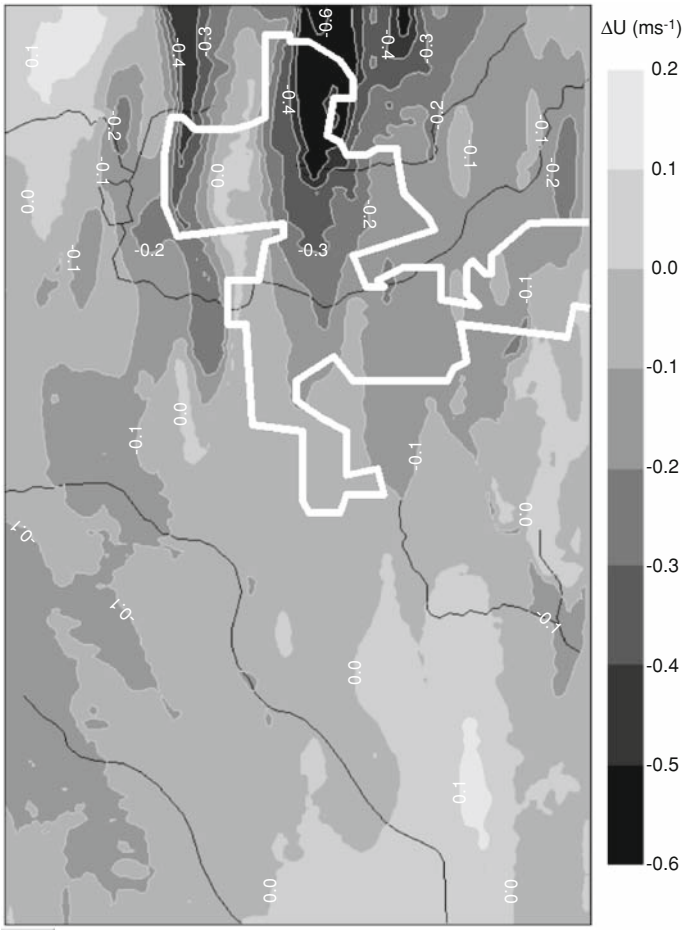

Fig. 15 Difference of maximum horizontal wind speed between *Urban* and *No Urban* on July 26 at 2200 LST. The OKC city limits are indicated by the *thick black line*

conditions as well as the large air temperatures, seem to be predominant in this particular case. The urban effects are more important at night when they are strongly coupled with the nocturnal south-westerly LLJ present across the Great Plains. The street-level nocturnal UHI vertically extends throughout the first hundred metres of the atmosphere above OKC, and tends to reinforce the large-scale horizontal temperature gradient already induced by the LLJ above and downwind of the city. The characteristics of the flow are also affected by the city; the large roughness of the urban covers decelerates the flow near the surface and reduces the maximum wind speed of the LLJ. In addition, the LLJ slightly rises above and downstream of OKC.

Results presented in this study shed new light on atmospheric boundary-layer processes over cities, and particularly underline the major role played by the nocturnal LLJ in the OKC area. Although it is influenced near the surface by the city, the LLJ is at the origin of the less stable layer observed at night in the first 200 m above OKC. Comparison of model results with upper-air observations shows that some processes remain difficult to accurately simulate,

in particular the transition periods leading to the development and breakdown of the LLJ, but also the complex multi-layer structure observed in vertical temperature and wind profiles.

Acknowledgements The authors are grateful to Bernard Bilodeau, Pierre Pellerin, Lubos Spacek, and Vivian Lee for their technical assistance in the development of the numerical modelling system, and to Gianpaolo Balsamo for his help in the application of the CaLDAS system to this study. Thanks are also due to Linying Tong, Najat Benbouta, Radenko Pavlovic who were involved in the data analysis. The support of the Meteorological Service of Canada management, in particular Gilbert Brunet and Richard Hogue, is warmly acknowledged. This work is funded by the Chemical, Biological, Radiological and Nuclear (CBRN) Research and Technology Initiative (CRTI) (Project #02-0093RD) of Defence R&D Canada.

References

Allwine KJ, Leach MJ, Stockham LW, Shinn JS, Hosker RP, Bowers JF, Pace JC (2004) Overview of Joint Urban 2003—an atmospheric dispersion study in Oklahoma City. In: Planning, nowcasting, and forecasting in the urban zone symposium, 84th AMS annual meeting, Seattle, WA, USA

Balsamo G, Mahfouf J-F, Bélair S, Deblonde G (2007) A land data assimilation system for soil moisture and temperature: an information content study. J Hydrometeorol 8(6):1225–1242

Bejarán RA, Camilloni IA (2003) Objective method for classifying air masses: an application to the analysis of Buenos Aires' (Argentina) urban heat island intensity. Theor Appl Climatol 74:93–103

Bélair S, Crevier L-P, Mailhot J, Bilodeau B, Delage Y (2003) Operational implementation of the ISBA land surface scheme in the Canadian regional weather forecast model. Part I: Warm season results. J Hydrometeorol 4:352–370

Berg LK, De Wekker SFJ, Shaw WJ, Allwine KJ (2004) Observations of boundary-layer winds in an urban environment. In: 5th AMS symposium on urban environment, American Meteorological Society, Vancouver, BC, Canada

Blackadar AK (1957) Boundary layer wind maxima and their significance for the growth of nocturnal inversions. Bull Am Meteorol Soc 38(5):283–290

Blackadar AK (1962) The vertical distribution of wind and turbulent exchange in a neutral atmosphere. J Geophys Res 67:3095–3102

Bleeker W, André J (1951) On the diurnal variation of precipitation, particularly over centural U.S.A., and its relation to large-scale orographic circulation systems. Q J Roy Meteorol Soc 77:260–271

Bonner WD (1968) Climatology of the low level jet. Mon Weather Rev 96(12):833–850

Bornstein R, Lin Q (2000) Urban heat islands and summertime convective thunderstorms in Atlanta: three case studies. Atmos Environ 34:507–516

Calhoun R, Heapa R, Princevacb M, Newsomc R, Fernandod H, Ligon D (2007) Virtual towers using coherent Doppler lidar during the Joint Urban 2003 dispersion experiment. J Appl Meteorol Climatol 45(8): 1116–1126

Chow W, Roth M (2006) Temporal dynamics of the urban heat island of Singapore. Int J Climatol 26(15):2243–2260

Danko DM (1992) The digital chart of the world. GeoInfo Syst 2:29–36

De Wekker SFJ, Berg LK, Allwine KJ, Doran JC, Shaw WJ (2004) Boundary-layer structure upwind and downwind of Oklahoma City during the Joint Urban 2003 field study. In: 5th AMS symposium on urban environment, American Meteorological Society, Vancouver, BC, Canada

Delage Y (1997) Parameterising sub-grid scale vertical transport in atmospheric models under statically stable conditions. Boundary-Layer Meteorol 82:23–48

Delage Y, Girard C (1992) Stability functions correct at the free convection limit and consistent for both the surface and Ekman layers. Boundary-Layer Meteorol 58:19–31

Erfani A, Mailhot J, Gravel S, Desgagné M, King P, Sills D, McLennan N, Jacob D (2005) The high resolution limited area version of the global environmental multiscale model and its potential operational applications. In: 11th conference on mesoscale processes, American Meteorological Society, Albuquerque, NM, USA

Fan H, Sailor DJ (2005) Modeling the impacts of anthropogenic heating on the urban climate of Philadelphia: a comparison of implementations in two PBL schemes. Atmos Environ 39(1):73–84

Fast JD, Torcolini JC, Redman R (2005) Pseudovertical temperature profiles and the urban heat island measured by a temperature datalogger network in Phoenix, Arizona. J Appl Meteorol 44:3–13

Figuerola PI, Mazzeo NA (1998) Urban-rural temperature differences in Buenos Aires. Int J Climatol 18: 1709–1723

Gedzelman SD, Austin S, Cermak R, Stefano N, Partridge S, Quesenberry S, Robinson DA (2003) Mesoscale aspects of the urban heat island around New York City. Theor Appl Climatol 75(1–2):29–42
Heap RB, Calhoun R, Princevac M, Sommer J (2004) Lidar measurements of atmospheric flow through a downtown cluster of high-rise buildings. In: 5th AMS symposium on urban environment, American Meteorological Society, Vancouver, BC, Canada
Helfand HM, Schubert SD (1995) Climatology of the simulated Great Plains low-level jet and its contribution to the continental moisture budget of the United States. J Clim 8:784–806
Hidalgo J, Masson V, Pigeon G (2008) Urban-breeze circulation during the CAPITOUL experiment: numerical approach. Meteorol Atmos Phys 102(3–4):243–262
Kim YH, Baik JJ (2005) Spatial and temporal structure of the urban heat island in Seoul. J Appl Meteorol 44:591–605
Lemonsu A, Masson V (2002) Simulation of a summer urban breeze over Paris. Boundary-Layer Meteorol 104:463–490
Lemonsu A, Grimmond CSB, Masson V (2004) Modelisation of the surface energy budget of an old Mediterranean city core. J Appl Meteorol 43:312–327
Lemonsu A, Pigeon G, Masson V, Moppert C (2006a) Sea-town interaction over Marseille: 3D urban boundary layer and thermodynamic fields near the surface. Theor Appl Climatol 84(1–3):171–178
Lemonsu A, Bastin S, Masson V, Drobinski P (2006b) Vertical structure of the urban boundary layer over Marseille under sea-breeze conditions. Boundary-Layer Meteorol 118(3):477–501
Lemonsu A, Leroux A, Bélair S, Trudel S, Mailhot J (2006c) A general methodology of urban cover classification for atmospheric modelling. In: 6th symposium on the urban environment, American Meteorological Society, Atlanta, GA, USA
Lenderink G, Holtslag AAM (2004) An updated lengthscale formulation for turbulent mixing in clear and cloudy boundary layers. Q J Roy Meteorol Soc 130:3405–3427
Liu Y, Chen F, Warner T, Basara J (2006) Verification of a mesoscale data-assimilation and forecasting system for the Oklahoma City area during the Joint Urban 2003 field project. J Appl Meteorol Climatol 4(7):912–929
Loveland TR, Reed BC, Brown JF, Ohlen DO, Zhu Z, Yang L, Merchant JW (2000) Development of a global land cover characteristics database and IGBP DISCover from 1 km AVHRR data. Int J Remote Sens 21(6–7):1303–1330
Lundquist JK, Mirocha JD (2006) Interaction of nocturnal low-level jets with urban geometries as seen in Joint URBAN 2003 data. In: 6th symposium on the urban environment, American Meteorological Society, Atlanta, GA, USA
Mailhot J, Bélair S, Lefaivre L, Bilodeau B, Desgagné M, Girard C, Glazer A, Leduc A-M, Methot A, Patoine A, Plante A, Rahill A, Robinson T, Talbot D, Tremblay A, Vaillancourt P, Zadra A, Qaddouri A (2006) The 15-km version of the Canadian regional forecast system. Atmos Ocean 44(2):133–149
Martilli A, Clappier A, Rotach MW (2002) An urban surface exchange parameterization for mesoscale models. Boundary-Layer Meteorol 104:261–304
Masson V (2000) A physically-based scheme for the urban energy budget in atmospheric models. Boundary-Layer Meteorol 94:357–397
Masson V, Grimmond CSB, Oke TR (2002) Evaluation of the Town Energy Balance (TEB) scheme with direct measurements from dry districts in two cities. J Appl Meteorol 41:1011–1026
Mitchell MJ, Arritt RW, Labas K (1995) A climatology of the warm season Great Plains low-level jet using wind profiler observations. Weather Forecast 10:576–591
Noilhan J, Planton S (1989) A simple parameterization of land surface processes for meteorological models. Mon Weather Rev 117:536–549
Oke TR (1987) Boundary layer climates, 2nd edn. Methuen, London, 435 pp
Peagle J, Peagle N, McCorcle M, Miller E (1984) Diagnoses and numerical simulation of a low-level jet during ALPEX. Beitr Phys Atmos 57:419–430
Pearlmutter D, Bitan A, Berliner P (1999) Microclimatic analysis of "compact" urban canyons in an arid zone. Atmos Environ 33(10):4143–4150
Pigeon G, Legain D, Durand P, Masson V (2007) Anthropogenic heat release in an old European agglomeration (Toulouse, France). Int J Climatol 27(14):1969–1981
Rosenzweig C, Solecki WD, Parshall L, Chopping M, Pope G, Goldber R (2005) Characterizing the urban heat island in current and future climates in New Jersey. Environ Hazards 6:51–62
Sarrat C, Lemonsu A, Masson V, Guedalia D (2006) Impact of urban heat island on regional atmospheric pollution. Atmos Environ 40(10):1743–1758
Song J, Liao K, Coulter RL, Lesht BM (2005) Climatology of the low-level jet at the Southern Great Plains atmospheric boundary layer experiments site. J Appl Meteorol 44:1593–1606

Steinecke K (1999) Urban climatological studies in the Reykjavík subarctic environment Iceland. Atmos Environ 33:4157–4162

Wang Y, Garvey DM, Klipp CL, Ligon DA, Williamson CC, Chang SS, Huynh GD, Calhoun R (2005) Low-level jet dominated atmospheric boundary layer observed by Doppler lidars over Oklahoma City during JU2003. In: Battlespace atmospheric and cloud impacts on military operations (BACIMO) conference, Monterey, CA, USA